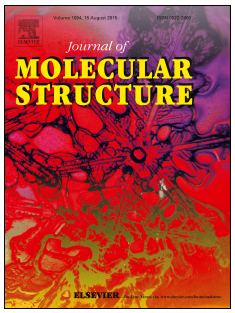

Synthesis of a novel phenytoin derivative: Crystal structure, Hirshfeld surface analysis and DFT calculations

Walid Guerrab, Hassane Lgaz, Sevgi Kansiz, Joel T. Mague, Necmi Dege, M. Ansar, Riadh Marzouki, Jamal Taoufik, Ismat H. Ali, Min Chung, Ill, Youssef Ramli

PII: S0022-2860(19)31739-9

DOI: https://doi.org/10.1016/j.molstruc.2019.127630

Reference: MOLSTR 127630

To appear in: *Journal of Molecular Structure*

Received Date: 19 September 2019

Revised Date: 16 December 2019

Accepted Date: 19 December 2019

Please cite this article as: W. Guerrab, H. Lgaz, S. Kansiz, J.T. Mague, N. Dege, M. Ansar, R. Marzouki, J. Taoufik, I.H. Ali, M. Chung Ill., Y. Ramli, Synthesis of a novel phenytoin derivative: Crystal structure, Hirshfeld surface analysis and DFT calculations, *Journal of Molecular Structure* (2020), doi: https://doi.org/10.1016/j.molstruc.2019.127630.

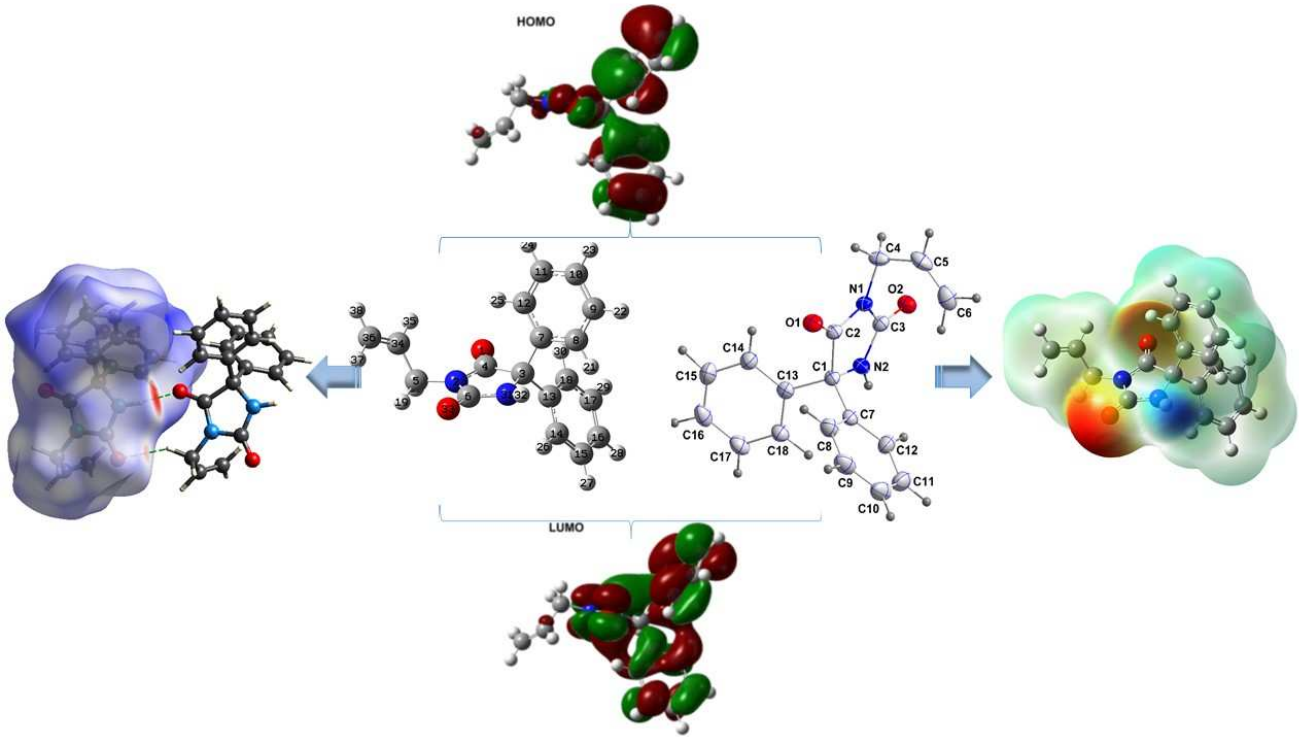

Synthesis of a novel Phenytoin Derivative: Crystal Structure, Hirshfeld Surface Analysis and DFT calculations

Walid Guerrab[1,a], Hassane Lgaz[2,a], Sevgi Kansiz[3], Joel T. Mague[4], Necmi Dege[3], M. Ansar[1], Riadh Marzouki[5,6,7], Jamal Taoufik[1], Ismat H. Ali[5], Ill-Min Chung[2*], and Youssef Ramli[1*]

[1]Laboratory of Medicinal Chemistry, Drug Sciences Research Center, Faculty of Medicine and Pharmacy, Mohammed V University, Rabat, Morocco.
[2]*Department of Crop Science, College of Sanghur Life Science, Konkuk University, Seoul 05029, South Korea.*
[3]Ondokuz Mayıs University, Faculty of Arts and Sciences, Department of Physics, 55139, Kurupelit, Samsun, Turkey.
[4]Department of Chemistry, Tulane University, New Orleans, LA 70118, USA.
[5]Chemistry Department, College of Science, King Khalid University, Abha 61413, Saudi Arabia.
[6]Laboratory of Materials, Crystal Chemistry and Applied Thermodynamics, LR15ES01, Faculty of Sciences of Tunis, University of Tunis El Manar, 2092, Tunisia.
[7]Chemistry Department, Faculty of Sciences of Sfax, University of Sfax, 3038, Tunisia.

*Corresponding authors:
Youssef Ramli, Email: **y.ramli@um5s.net.ma**
Ill-Min Chung, Email: **imcim@konkuk.ac.kr**
[a]Have equal contribution in this work

Abstract

Hydantoin compounds are important heterocyclic scaffolds and a class of well-known bioactive molecules with a broad spectrum of pharmacological properties. Consequently, considerable efforts have been devoted to the design and synthesis of a broad range of hydantoin derivatives. In this context, the compound 3-allyl-5,5-diphenylimidazolidine-2,4-dione, $C_{18}H_{16}N_2O_2$ (3ADID) was synthesized and its structure was determined by X-ray structure analysis. Further, the molecular structure was examined using Hirshfeld topology analysis and Density Functional Theory

(DFT)-B3LYP calculations with the basis set 6-311++G (d,p). In the title molecule, $C_{18}H_{16}N_2O_2$, the imidazolidine ring is planar with the allyl substituent oriented nearly perpendicular to it. In the crystal, hydrogen bonded chains of molecules are arranged in sets of three about the 3_2 axes by C—H···π (ring) interactions. Hirshfeld surface map and 2D fingerprint plots were used to explore intermolecular interactions. The optimized geometry, global reactivity descriptors, and HOMO-LUMO orbitals of the molecule were computed by DFT and discussed. To evaluate the chemical reactivity and charge distribution on the molecule, molecular electrostatic potential (MEP) and atomic charges, computed by Mulliken population analysis and NBO theory were determined. The local reactivity was examined by determining the Fukui functions and dual descriptor indices. DFT calculations at the same level of theory, with the POP=NBO keyword, were used to evaluate charge delocalization and hyperconjugative interactions through Natural Bond orbital analysis.

Keywords: Crystal structure; DFT; XRD; Phenytoin; Fukui function; Hirshfeld surface.

1. Introduction

Imidazolidine-2,4-diones, known as Hydantoins, are among the privileged chemical scaffolds utilized in the development of anticonvulsant drugs [1]. It is a popular scaffold in the design of several pharmaceutical compounds as well as in natural products and organic synthesis [2,3]. For example, phenytoin is a hydantoin derivative and it is one of the oldest and well-known non-sedative antiepileptic drugs [4]. It is the widely used anticonvulsant for treating acute convulsive seizures [5]. It is also applicable for various diseases, as it has antiarrhythmic, and anti-HIV [6,7], anti-

diabetes, and anti-anxiety effects among others [8]. The antiproliferative [9] and cytotoxic [10] activities of the cycloalkanspiro-5-hydantoins have also been reported. Moreover, chemical modifications of imidazolidine-2,4-dione by alkylation allow researchers to enrich its chemical structure, thus strengthening and extending its biological activity. Consequently, several recently developed hydantoin derivatives have a wide spectrum of pharmacological and biological activities, such as isocitrate dehydrogenase inhibitors [11], anti-inflammatory [12,13], Anti-fibrolytic [14,15], antibacterial [16], antidiabetic [17], kinesin spindle protein inhibitors [18], antiplatelet [19], and antimalarials [20] activities. Besides these vast pharmacological and biological properties, hydantoin derivatives have also shown to be good corrosion inhibitors [21].

Our research group has more recently reported the synthesis of a novel thiohydantoin-based compound [22]. In continuation of our efforts toward the discovery of novel hydantoin-based compounds [23–25], herein, we hereby present the synthesis of a novel phenytoin derivative, namely, 3-allyl-5,5-diphenylimidazolidine-2,4-dione (3ADID). Characterization of its molecular structure was carried out by X-ray crystallography, Hirschfeld surfaces analysis and DFT-B3LYP method with the basis set 6-311++G (d,p). The frontier molecular orbitals (FMOs) and chemical reactivity descriptors were examined to evaluate the reactivity of the synthesized compound. Local reactivity (Fukui functions), Molecular electrostatic potential (MEP) and net charges (NBO&MPA) were also calculated and discussed. NBO analysis was performed to calculate the net electron transfer from the donor to acceptor.

2. Experimental section

2.1. General information

Mass spectra are recorded in a SYNAPT G2 HDMS (Waters) Spectrometer in electrospray ionization (ESI). Infrared spectra were recorded on a Perkin Elmer 577, using KBr disks. ^{1}H NMR and ^{13}C NMR spectra were recorded on Bruker Avance 300NMR Spectrometer in DMSO-d_6. Spectra were internally referenced to TMS. Peaks are reported in ppm downfield of TMS.

2.2. Synthesis

Synthesis of 5,5-diphenylimidazolidine-2,4-dione: we have adopted the same procedure described in the literature [11], which first consists in preparing benzyl by oxidation of benzoin in present of copper sulfate, then the action of urea in ethanol at reflux with benzyl leads to the phenytoin with a good yield (Scheme 1).

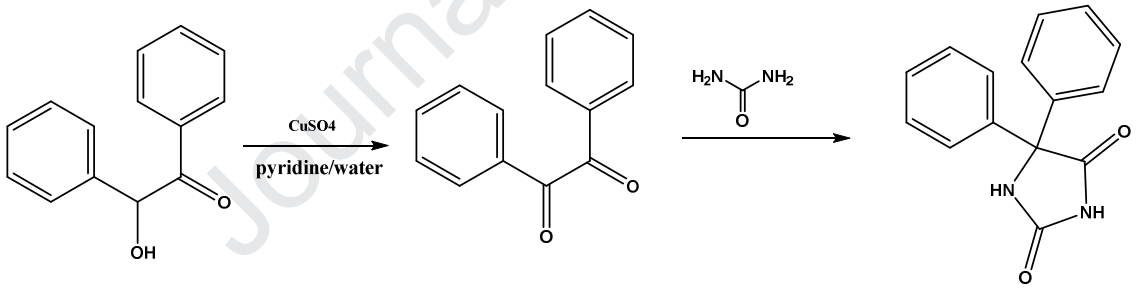

Scheme 1: Synthesis procedure for preparation of 5,5-diphenylimidazolidine-2,4-dione.

Synthesis of 3-allyl-5,5-diphenylimidazolidine-2,4-dione: Alkylation reaction using the appropriate bromide allyl was carried out under phase transfer catalysis (PTC) to prepare the title compound, and added to a solution of 5,5- diphenylhydantoin in DMF, potassium carbonate and tetra-n-butylammonium bromide (scheme 2). The

synthesized 3ADID has been characterized by single crystal X-ray structure analysis (Fig. 1).

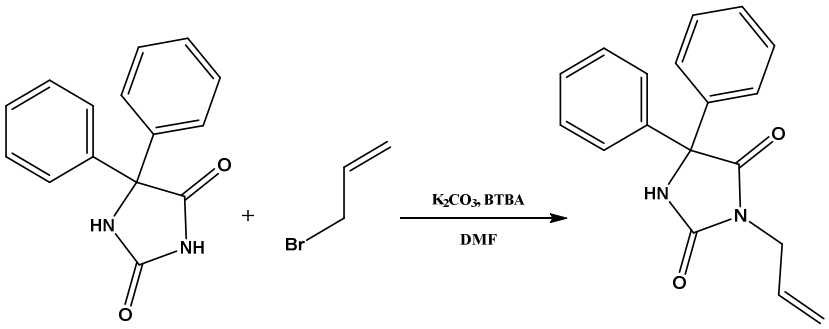

Scheme 2: Synthesis procedure for preparation of 3-allyl-5,5-diphenylimidazolidine-2,4-dione (3ADID).

HRMS (ESI) [M+ H]: m/z=293.1

[M+ Na]: m/z=315.3

IR (v, cm^{-1}) : The IR spectra of imidazolidine-2,4-diones derivative showed bands in 3268 cm^{-1} region for the NH lactamic functional group 1765-1698 cm^{-1} for the C=O functional group, and 3086-3060 cm^{-1} for the C-H aromatic functional group. Moreover, IR spectra revel the disappearance of bands for NH in position 3 and the appearance of new bands 2986-3086cm^{-1} for aliphatic functional groups C-H.

NMR (400 MHz, DMSO) δ (ppm) : The ^{1}H NMR spectrum of the new synthetized compound was characterized by the presence of multiple signals at: 5.745-5.837 ppm corresponding for $CH=CH_2$ proton, a double doublet signals corresponding of $CH=CH_2$ of the aliphatic chains and a quartet signals at 4.020-4.037 ppm was observed for the methyl protons directly connected to nitrogen atom. Beside the latter three aliphatic signals, the ^{1}H NMR spectrum of the compound exhibited a multiple signals for aromatic protons at: 7.402-7.1967 ppm with ten proton integral

value which are assigned to protons at C-2,6, C-3,5 and C-4 carbons of phenyls. The singlet signal at 9.691 ppm is assigned for the NH proton.

^{13}C NMR (on-resonance & DEPT) spectral assignment of the obtained product has been made. ^{13}C NMR spectra of the studied compound displayed the expected signals for the 5,5-diphenyl imidazolidine-2,4-diones core at 173.290-155.414 ppm for **C**=O, 140.096 ppm for **C**q position 5. The aromatic carbons could be readily distinguished from the other carbons due to their characteristic absorption.13C NMR at 129.257, 129.079, 128.672. Spectrum showed three signals in the alkene region. The signal at 132.494 ppm for aliphatic **C**H, at 128.672 ppm for (**C**H_2=), and a signal at 116.710 ppm due to N-**C**H_2 group. All spectrums are shown in supplementary material.

2.3. Single crystal XRD study

Data collection of $C_{18}H_{16}N_2O_2$ was performed using a Bruker D8 VENTURE PHOTON 100 CMOS diffractometer equipped with a mirror monochromatic Cu-Kα radiation (λ = 1.54178 Å) produced by an Incoatec IμS micro focus source. The structure solution was solved by means of SHELXT [26] and refinements were carried out on F^2 by full-matrix least-squares techniques using SHELXL [26]. The experimental details including structure refinement and data collection details for $C_{18}H_{16}N_2O_2$ were summarized in Table 1.

Table 1. Crystal data and structure refinement parameters for 3-allyl-5,5-diphenylimidazolidine-2,4-dione (3ADID).

Chemical formula	$C_{18}H_{16}N_2O_2$
CCDC deposition number	1947113

Formula weight	292.33
Temperature (K)	150
Crystal system, space group	Trigonal, $P3_2$
Unit cell dimensions	
a, c (Å)	14.5779 (3), 6.1846 (2)
V ($Å^3$)	1138.24 (6)
Z	3
Radiation type	Cu Kα
μ (mm−1)	0.68
Crystal size (mm)	0.26 × 0.12 × 0.11
Data collection	
Diffractometer	Bruker D8 VENTURE PHOTON 100 CMOS
Absorption correction	Multi-scan SADABS [27]
Tmin, Tmax	0.84, 0.93
No. of measured, independent and observed [I > 2σ(I)] reflections	5649, 2936, 2858
R_{int}	0.032
(sin θ/λ)max (Å−1)	0.618
Refinement	
R[F2 > 2σ(F2)], wR(F2), S	0.027, 0.065, 1.05
No. of reflections	2936
No. of parameters	264
No. of restraints	1
H-atom treatment	H-atom parameters constrained
Δρmax, Δρmin (e Å−3)	0.12, −0.11
Absolute structure	Flack x determined using 1335 quotients [(I+)-(I-)]/[(I+)+(I-)][28].
Absolute structure parameter	0.01 (10)

2.4. Hirshfeld surface analysis

In order to obtain visualization of intermolecular interactions in 3-allyl-5,5-diphenylimidazolidine-2,4-dione, Hirshfeld surface analysis was carried out. Both the Hirshfeld surface [1] and 2D fingerprint [2] plots were generated using *CrystalExplorer17.5* program [3]. The structural input file was obtained in the CIF format. Hirshfeld surface was represented by d_e and d_i, which denote, respectively, the distance from the nearest atom outside and inside of the surface and both are used to define the normalized contact distance (d_{norm}). For the visualization of d_{norm}, a red-blue-white (RBW) color scale was selected.

2.5. Quantum chemical calculations

All DFT computations were performed using Gaussian 09W package [29]. GaussView molecular visualization software was used to draw the initial structure and to visualize the results [30]. The molecular structure of the 3ADID was optimized using DFT-B3LYB method with the basis set 6-311++G (d,p), default SCF and geometrical convergence criteria in the gas phase [31–33]. Information about delocalization of charge in the synthesized compound was provided through NBO analysis using NBO Ver. 3.1 (Implemented in Gaussian Software) at the same DFT level with the POP=NBO keyword. Chemical reactivity of the compound was discussed in view of the global reactivity descriptors and HOMO-LUMO energies. MEP, natural charges and Mulliken charges were determined to investigate the charge distribution on the molecule. Electrophilicity and nucleophilicity theoretical descriptors were investigated by performing Fukui functions calculation using the GGA functional according to Perdew, Burke and Ernzerhof (PBE) and the DNP basis set [34] packed in Dmol3 module of Materials Studio (MS) software [35].

3. Results and discussions

3.1. Description of the crystal structure of 3ADID

The imidazolidene ring is planar with the allyl substituent oriented nearly perpendicular to it. In the crystal hydrogen bonded chains of molecules are arranged in sets of three about the 32 axes by C—H···π(ring) interactions.The phenyl rings are inclined to the mean plane of the imidazolidene ring by approximately equal amounts. In the crystal, N—H···O and C—H···O form chains extending along the c-axis direction which are combined into sets of three by helical motifs of C—H···π(ring) interactions.

The C7···C12 and C13···C18 benzene rings, respectively, are inclined to the mean plane of the 5-membered ring by 62.08 (7) and 64.55 (7)°. The 5-membered ring is planar to within 0.0314 (11) Å (rms deviation of the fitted atoms = 0.0036) with C2 showing the largest deviation from the mean plane. The allyl group is oriented nearly perpendicular to this plane as indicated by the C3—N1—C4—C5 torsion angle of -83.9 (3)°. In the crystal, the molecules form chains extending along the c-axis direction through N2—H2···O1 and C4—H4B···O2 hydrogen bonds (Table 2 and Fig. 2). Sets of three chains surrounding the 32 axes are linked by sets of C16—H16···Cg3 interactions having a helical motif (Table 2 and Fig. 3).

Table 2. Hydrogen-bond geometry (Å, °)

Cg3 is the centroid of the C13···C18 ring.

D—H···*A*	*D*—H	H···*A*	*D*···*A*	*D*—H···*A*
N2—H2···O1^{i}	0.90 (3)	1.94 (3)	2.834 (2)	170 (2)
C4—H4B···O2^{ii}	0.95 (3)	2.52 (3)	3.322 (2)	143 (2)
C16—H16···Cg3^{iii}	0.98 (3)	2.98 (4)	3.791 (3)	141 (3)

Symmetry codes: (i) *x*, *y*, *z*+1; (ii) *x*, *y*, *z*−1; (iii) −*x*+*y*+1, −*x*+1, *z*+1/3.

3.2. Optimized molecular structure by X-Ray crystallography and DFT

The geometric structure of 3ADID optimized by using DFT at B3LYP/6-311G++ (d,p) level is shown in Fig. 4. Based on DFT and XRD studies, selected geometrical parameters were determined and listed in Table 3. The results of DFT and XRD are almost identical and a comparison between both results indicates that there are only minor deviations, which is mainly due to differences in the molecular environment [36] since the molecular structure of 3ADID was investigated by X-ray crystallography in the crystalline phase, whereas DFT calculations of isolated molecule were performed in the gas phase. In X-ray structure, the N1-C2, N1-C3, N2-C1, and N2-C3 bond lengths are 1.352(2), 1.412(2), 1.458(2) and 1.351(2) Å, whereas in DFT-optimized geometry, the calculated values are 1.36429, 1.41180, 1.45961, and 1.36643 Å, respectively. These values demonstrate a good agreement between them. Similarly, N1-C4-C5 (112.89(17)/112.85), N2-C1-C7 (112.91(15)/112.88) and C13-C1-C7 (110.18(15)/110.84) bond angle values computed from the DFT/X-ray crystallography are in close agreement. The most obvious difference in torsion angle values occurs at N2-C1-C7-C8 torsion angle, with the difference in the value being of 8.51°. In general, despite differences in the molec ular environment, good correlation was found between DFT and XR crystallography values.

Table 3. Some selected experimental and theoretical geometric parameters for 3-allyl-5,5-diphenylimidazolidine-2,4-dione (3ADID) (Å, ˚).

Geometric Parameters	**Experimental [X–ray diffraction]**	**Theoretical [DFT/B3LYB]**
Bond (Å)		
O1-C2	1.221(2)	1.21253
N1-C2	1.352(2)	1.36429
N1-C4	1.450(2)	1.46499

N2-C1	1.458(2)	1.45961
O2-C3	1.210(2)	1.21025
N1-C3	1.412(2)	1.41180
N2-C3	1.351(2)	1.36643
C1-C13	1.530(3)	1.53721
C1-C2	1.538(2)	1.55676
C5-C6	1.307(4)	1.33243
C7-C12	1.391(3)	1.39824
C8-C9	1.390(3)	1.39340
C9-C10	1.392(4)	1.39779
C10-C11	1.376(4)	1.39432
C11-C12	1.397(3)	1.39796
C13-C18	1.398(3)	1.40381
C1-C7	1.534(3)	1.53633
C4-C5	1.494(3)	1.50764
C7-C8	1.392(3)	1.40292
C13-C14	1.386(3)	1.39944
C14-C15	1.393(3)	1.39773
C15-C16	1.375(4)	1.39434
C16-C17	1.387(3)	1.39721
C17-C18	1.385(3)	1.39374
Bond angles (º)		
C2-N1-C3	111.89(14)	112.44977
C3-N1-C4	122.71(15)	122.98799
N2-C1-C13	110.64(14)	110.26729
C13-C1-C7	110.18(15)	110.84643
O1-C2-N1	126.57(17)	125.98273
N1-C2-C1	107.44(14)	106.98941
O2-C3-N1	124.52(16)	125.56565
N1-C4-C5	112.89(17)	112.85208
C8-C7-C1	119.31(17)	119.02032
C18-C13-C1	117.56(16)	118.15902
C2-N1-C4	125.40(15)	124.44698
C3-N2-C1	113.39(15)	113.21870
N2-C1-C7	112.91(15)	112.88016
N2-C1-C2	100.42(14)	100.49177
O1-C2-C1	125.97(17)	127.02738
O2-C3-N2	128.91(17)	128.20371
N2-C3-N1	106.57(15)	106.21940
C12-C7-C1	120.89(18)	121.75268
C14-C13-C1	123.33(17)	122.92036
Torsion angles (º)		
C3-N2-C1-C13	124.48(16)	-121.41418
C4-N1-C2-C1	-174.99(17)	179.52381
C4-N1-C3-N2	177.24(17)	176.54569
C1-C7-C12-C11	-177.36(19)	179.33481
C3-N1-C2-O1	-176.48(18)	-176.90189
N2-C1-C2-O1	176.55(18)	-178.18573
C13-C1-C2-N1	-123.56(16)	119.93976
C1-N2-C3-O2	178.92(19)	-172.78462

C2-N1-C3-O2	177.29(18)	173.93619
N2-C1-C7-C8	170.54(16)	-179.05444
C1-C7-C8-C9	178.45(19)	-176.11034
C7-C1-C13-C14	129.00(19)	129.36833
C2-C1-C13-C18	-177.08(16)	-176.17660
C1-C13-C14-C15	176.4(2)	176.34060
C1-C13-C18-C17	-176.02(19)	-176.11034

Numbering is according to Fig. 4.

3.3. Molecule's reactivity analysis by global reactivity descriptors

Frontier molecular orbitals (FMOs), i.e. HOMO and LUMO, are the most important orbitals in a molecule. They are a well-known analysis to investigate the reactive ability of compounds [37–40]. They determine the ability of a compound to accept (in the case of LUMO) or donate (in the case of HOMO) an electron [39,41,42]. HOMO and LUMO orbitals of the title compound were examined and are shown in Fig. 5. The electronic distribution reflects the donor-acceptor capabilities of the molecular structure. Accordingly, both HOMO and LUMO orbitals are located over the two phenyls and the hydantoin moiety. The well-defined electron density map for 3ADID reflects its good interactive ability.

By using the energies of FMOs, the ionization energy (IP) and electron affinity (EA) can be determined by the following formulas [43]:

$$EA = -E_{\mathrm{LUMO}} \quad (1)$$

$$IP = -E_{\mathrm{HOMO}} \quad (2)$$

The chemical potential (μ), absolute electronegativity (χ) and absolute hardness (η) were calculated from combination of ionization energy and electron affinity values using the following equations [43]:

$$\chi = -\mu = \frac{IP + EA}{2} \quad (3)$$

$\eta = \frac{IP - EA}{2}$ (4) and $\sigma = \frac{1}{\eta}$ (5) denotes the softness (σ).

Recently, Serdaroğlu and Ortiz have reported quantum chemical calculations for phenytoin [44]. Therefore, in order to investigate the effect of alkylation on the reactivity and electronic properties of 3ADID, it is instructive to compare their results with ours. Quantum chemical parameters of phenytoin and 3ADID are reported in Table 4. A large E_{HOMO} value indicates a higher tendency to donate electrons, whereas, in contrast, a lower E_{LUMO} value indicates a higher ability to accept electrons [45,46]. The HOMO-LUMO gap (ΔE), on the other hand, is an important stability index. If its value is higher, it indicates higher stability, and vice versa if its value is lower [45,47]. Based on results in Table 4, 3ADID compound has a more tendency to give its electrons while phenytoin tends to accept electrons. In terms of the gap value, there is a low value for the phenytoin molecule compared to 3ADID. The η and σ values of 3ADID are, respectively 2.979 eV and 0.336 eV^{-1} and those of phenytoin are, respectively 2.936 eV and 0.340 eV^{-1}. These results indicate that the phenytoin became harder after its alkylation. It is well known that molecules with smaller energy gap are in most case softer than those with a large energy gap (which is the case here).

The electrophilicity index (ω) and its multiplicative inverse i.e. the nucleophilicity index (ε) were calculated using the following formulas [48,49]:

$$\omega = \frac{\mu^2}{2\eta} \quad (6)$$

$$\varepsilon = \frac{1}{\omega} \quad (7)$$

The electrophilicity is a good indicator of the electron-accepting ability, whereas molecules having a large nucleophilicity are known to have strong ability to accept

electron [50]. In our results, phenytoin is found to be strongest electrophile whereas the synthesized phenytoin derivative (3ADID) is the strongest nucleophile.

Table 4. Quantum chemical parameters of 3-allyl-5,5-diphenylimidazolidine-2,4-dione obtained by DFT-B3LYB.

Parameter	Value	
	3ADID	Phenytoin [44]
E_{HOMO}, (eV)	-6.603	-7.061
E_{LUMO}, (eV)	-0.644	-1.188
ΔE, (eV)	5.959	5.873
IP, (eV)	6.603	7.061
EA, (eV)	0.644	1.188
Ƞ, (eV)	2.979	2.936
χ, (eV)	3.624	4.124
ω, (eV)	2.203	2.896
σ, (eV^{-1})	0.335	0.340
ε, (eV-1)	0.453	0.345

3.4. Molecular electrostatic potential analysis

The MEP map is a visual tool to understand the relative polarity and predict reactive sites of a molecule [38]. It is associated with the electronic cloud and it is an important descriptor in evaluating the potential electrophilic and nucleophilic regions in a molecule [51]. In this work, the MEP mapping was calculated by DFT-B3LYB method as shown in Fig. 6 to visualize the charge distribution on the molecule. The area with dark red color means potential that is more negative and that area in a molecule have more preference for electrophilic attacks, while the area with intense blue color indicates potential that is more positive and it is related to nucleophilic reactivity [22,38]. Intermediate electrostatic potentials are between red and blue potentials according to the following order: red < orange < yellow < green < blue.

From the MEP plot, it can been seen that negative electrostatic potentials are spread over the carbonyl oxygen atom, indicating possible sites for electrophilic attack while electropositive region is mainly localized over the protonated nitrogen atom.

3.5. Mulliken and NBO atomic charges

We have also computed Mulliken and NBO charges and results are listed in Table 5 and Fig. S1. The charge distribution over the atoms was found to be significant in describing donor and acceptor pairs and to get insights into the overall activity of the compound [22]. Moreover, it would be very interesting to compare these results with those of similar compounds, especially to show the effect of substitution of the hydantoin moiety on the charge distribution. The computed results reveal that only C4, C6, C7 and C13 (Mulliken charges) and C3, C4 and C6 (NBO charge) exhibit a positive charge whereas all other atoms exhibit negative charges. The O1 (-0.427346) and O33 (-0.425187) atoms have the maximum negative Mulliken charges, while the N31 atom has the highest negative NBO charge, followed by O33 and O1 atoms. This is compatible with results of Nogueira et al. who found that both oxygen atoms are the most electronegative atoms in 1-methylhydantoin molecule [52]. The nitrogen atoms N2 and N31 have negative total charges because of their strong electronegativity as compared to carbon atoms to which they are attached; and the same results were found by Nogueira et al. for 5-methylhydantoin and 1-methylhydantoin molecules [52,53]. The results showed, unsurprisingly, that the maximum positive NBO charges are obtained for C4 and C6 (0.70418 and 0.81564, respectively) because they are connected to more electronegative atoms, i.e. oxygen and nitrogen. Overall, these results indicate that the hydantoin moiety plays an important role in the chemical reactivity of the synthesized compound.

Table 5. The Mulliken, natural atomic charge and the total negative charge (TNC) of 3-allyl-5,5-diphenylimidazolidine-2,4-dione obtained by DFT-B3LYB.

Atoms	Mulliken charges	NBO charges
1 O	-0.427346	-0.57466
2 N	-0.332549	-0.48537
3 C	-0.092554	0.04659
4 C	0.448394	0.70418
5 C	-0.091602	-0.30134
6 C	0.546891	0.81564
7 C	0.151390	-0.05175
8 C	-0.094742	-0.23213
9 C	-0.066158	-0.22885
10 C	-0.059768	-0.23372
11 C	-0.069822	-0.22625
12 C	-0.098379	-0.22496
13 C	0.135369	-0.05649
14 C	-0.101869	-0.23295
15 C	-0.064409	-0.23227
16 C	-0.061554	-0.23571
17 C	-0.071285	-0.23011
18 C	-0.070790	-0.21634
31 N	-0.392727	-0.67262
33 O	-0.425187	-0.59577
34 C	-0.005825	-0.24241
36 C	-0.187605	-0.41587
TNC	**-2.714171**	**-5.68957**

Numbering is according to Fig. 4.

3.6. Fukui functions

Identifying local reactivity parameters is among the most basic and commonly used tools to understand the reactivity and selectivity of a molecule [39]. The condensed Fukui functions, which resulted from a derivative of electron density keeping the positions of nuclei unchanged are a more practical and convenient way in predicting favorable sites for electrophilic or nucleophilic attack [22,54,55]. Nucleophilic,

electrophilic and radical attack are, respectively, expressed as (f^+), (f^-) and (f^0). They are defined as follows [56]:

$$f_k^+ = q_k(N+1) - q_k(N) \quad (8)$$

$$f_k^- = q_k(N) - q_k(N-1) \quad (9)$$

$$f_k^0 = \frac{1}{2}\left[q_k(N+1) - q_k(N-1)\right] \quad (10)$$

where q_k is the atomic charge at the k^{th} atomic site within a molecule in its neutral (N), anionic (N+1) or cationic (N-1) state [57].

The propensity toward nucleophilic or electrophilic attacks can be more precisely predicted by the dual descriptor, which is proposed by Morell et al. [58] and defined as:

$$\Delta f(k) = f_k^+ - f_k^- \quad (11)$$

In order to characterize the reactivity of an atomic site and to distinguish between electrophilic and nucleophilic attacks, the sign of the dual descriptor is mostly considered. The sites for electrophilic attack are marked with a positive sign of the dual descriptor while its negative sign means nucleophilic attack [51]. In the present study, condensed Fukui functions indices along with dual descriptor values of investigated molecule are listed in Table 6. Inspection of results in Table 6 shows that N1 and C9 atoms of both phenyls have a greater susceptibility to electrophilic attack (large values of f^- and negative Δf). In the case of the nucleophilic attack, C2, N3, C4, C5, O6, O7, C8, and C10 atoms have a higher propensity to nucleophilic attack (large values of f^+ and positive Δf). On the other hand, atoms that are more prone to radical attack are the C4, O6, O7, and C15. A closer inspection of results revealed

that the distribution of electrophilic and nucleophilic sites are in accordance with HOMO-LUMO orbitals.

Table 6. Condensed Fukui functions and dual descriptor of 3-allyl-5,5-diphenylimidazolidine-2,4-dione obtained by DFT-GGA.

Atom	f^0	f^+	f^-	Δf
N (1)	2.2	2	2.4	-0.4
C (2)	3.4	5.5	1.2	4.3
N (3)	2.4	3.8	1.1	2.7
C (4)	6.7	12.3	1	11.3
C (5)	1.3	1.8	0.8	1
O (6)	9.2	14.9	3.5	11.4
O (7)	5.6	8.5	2.7	5.8
C (8)	0.9	1.1	0.6	0.5
C (9)	0.4	0.2	0.6	-0.4
C (10)	1.4	1.7	1.1	0.6
C (11)	3.7	2.2	5.1	-2.9
C (12)	1.9	0.5	3.3	-2.8
C (13)	3.1	2.8	3.5	-0.7
C (14)	4.8	3.3	6.2	-2.9
C (15)	6.4	4.8	8	-3.2
C (16)	3.3	2.8	3.8	-1
C (17)	4.3	3.1	5.5	-2.4
C (18)	3.2	1.4	5	-3.6
C (19)	2.3	1.5	3	-1.5
C (20)	3.9	1.9	6	-4.1
C (21)	3.7	1.7	5.7	-4
C (22)	1.7	0.9	2.6	-1.7

Numbering is according to Fig. S2.

3.7. Donor-acceptor interactions by NBO analysis

The NBO analysis was performed to show the interaction between the donor NBO "filled" and acceptor NBO "virtual" in the molecule [41]. The NBO analysis is a sensitive tool for examining all possible interactions between filled Lewis-type NBOs (donors) and unoccupied non-Lewis NBOs (acceptors) and estimating their stabilization energy by the theory of 2nd order perturbations [39]. It allows

interpretation of hyperconjugative interaction or intermolecular delocalization result in the transfer of charge between vacant (antibonding or Rydgberg) and filled (bonding or lone pair) orbitals of two subsystems. The stabilization energy E(2), which is associated with electron delocalization between electron donor orbital *i* and electron acceptor orbital *j* reflects the extent of conjugation of the whole system. Larger E(2) means a stronger electron donor-acceptor interaction [59,60]. According to NBO analysis, the stabilization energy (E2) is computed from below formula [61]:

$$E(2) = -q_i \frac{F_{ij}^2}{\Delta E} = -q_i \frac{\langle i|F|j\rangle^2}{\varepsilon_j - \varepsilon_i} \quad (12)$$

where q_i is the donor orbital occupancy, ε_j, and ε_i are diagonal elements, F_{ij} is the off-diagonal NBO Fock matrix constituent.

For the title compound, some of the important donor-acceptor interactions (stabilization energy E (2) higher than 4 kcal/mol) are reported in Table S1 (Supplementary Material). The stabilization of the molecule is attained by the strong hyper-conjugative interaction of donors to acceptors. The results of the NBO analysis reveal that the most relevant donor-acceptor interactions are the interactions between the lone electron pair (LP) of the nitrogen atoms and the carbonyl bonds π antibonding orbitals. These are the same reported by Nogueira et al. in their NBO analysis of 5□methylhydantoin and 1-methylhydantoin molecules [52,53]. Lone pair around LP (1) N2 is distributed to π* anti-bonding O1-C4 and C6-O33 with stabilization energy of about 59.64 and 48.87 kcal/mol, respectively. Interestingly, similar interactions were reported by Nogueira et al. but with smallest stabilization energy [52,53]. Whereas, lone pair around LP (1) N31 is distributed to π* anti-bonding C6-O33 with stabilization energy of about 50.28 kcal/mol. Despite competition between the two interactions involving N2, the interaction energy for LP

(1) N31 → π* (C6-O33) is smaller than that corresponding to the LP (1) N2 → π*(O1-C4) orbital interaction, which is in contrast to what has been found by Nogueira et al. in their two studies [52,53].

Concerning other NBO interactions, the π electron delocalization is greater around C15-C16 bond and is dispersed to π* anti-bonding of C13-C14 and C17-C18 with energy 22.37 and 19.56 kcal/mol, respectively. The maximum stabilization energies 22.41 and 20.38 kcal/mol are due to the π electron delocalization about C17-C18 that is dispersed to π* anti-bonding of C13-C14 and C15-C16. In the case of intra molecular hydrogen bond, the significant interaction is occurred in σ(C36-H38) → σ* (C5-C34) (6.09 kcal/mol).

3.8. Hirshfeld surface analysis

Fig. 7 illustrates the Hirshfeld surface and the intermolecular contacts of the title compound mapped over d_{norm}. It was established that d_{norm} values vary from -0.5973 to +1.5340 a.u. The red regions (distances shorter than the sum of the van der Waals radii) is apparent around the oxygen atom (O2) participating in the C—H···O contacts and around the hydrogen atom (H2) participating in the N—H···O contacts in Fig. 7. The fingerprint plots are given in Fig. 8 for the title compound. The largest contribution to the overall crystal packing in the compound is from H···H interactions (54.8%). This significant contribution of H···H interactions to the total Hirshfeld surface was also reported in other studies [62,63]. C···H/H···C contacts are the second largest contribution to the Hirshfeld surface with 26.7%. The O···H/H···O contacts appear as a pair of characteristic tips in the fingerprint plots. O···H/H···O contacts contribute 15.9% to the Hirshfeld surface. Also, the O···H/H···O contacts

indicate the presence of intermolecular N—H···O and C—H···O interactions, respectively.

4. Conclusions

In the present work, a new phenytoin derivative, 3-allyl-5,5-diphenylimidazolidine-2,4-dione, formulated as $C_{18}H_{16}N_2O_2$ was synthesized and its structure was determined by X-ray crystallography. Further, the molecular structure was examined using Hirshfeld topology analysis and Density Functional Theory (DFT) at B3LYB/6-311++G(d,p) level. It was found that the compound crystallizes in the trigonal space group *P 32* with parameters a= 14.5779(3) Å, b= 14.5779(3) Å, c= 6.1846(2) Å, Z=3. Global and local descriptors of reactivity such as HOMO-LUMO and condensed Fukui functions along with net charges and MEP were used to evaluate the chemical reactivity of 3ADID. NBO analysis was performed for understanding the stability, intramolecular charge transfer and donor-acceptor interactions in the synthesized compound.

Conflict of interest:

The authors of this manuscript have no conflict of interest to declare.

Acknowledgements

“The authors extend their appreciation to the Deanship of Scientific Research at King Khalid University for funding this work through research groups program under grant number R.G.P.2/46/40.”

References

[1] M. Meusel, M. Gütschow, Recent developments in hydantoin chemistry. A review, Org. Prep. Proced. Int. 36 (2004) 391–443.
[2] S. Scholl, A. Koch, D. Henning, G. Kempter, E. Kleinpeter, The Influence of Structure and Lipophilicity of Hydantoin Derivatives on Anticonvulsant Activity, Struct. Chem. 10 (1999) 355–366. https://doi.org/10.1023/A:1022091411018.
[3] M. Mudit, M. Khanfar, A. Muralidharan, S. Thomas, G.V. Shah, R.W. van Soest, K.A. El Sayed, Discovery, design, and synthesis of anti-metastatic lead phenylmethylene hydantoins inspired by marine natural products, Bioorg. Med. Chem. 17 (2009) 1731–1738.
[4] N. Trišović, N. Valentić, G. Uščumlić, Solvent effects on the structure-property relationship of anticonvulsant hydantoin derivatives: A solvatochromic analysis, Chem. Cent. J. 5 (2011) 62. https://doi.org/10.1186/1752-153X-5-62.
[5] Y. Yaari, M.E. Selzer, J.H. Pincus, Phenytoin: Mechanisms of its anticonvulsant action, Ann. Neurol. 20 (1986) 171–184. https://doi.org/10.1002/ana.410200202.
[6] O. Werzer, R. Baumgartner, M. Zawodzki, E. Roblegg, Particular Film Formation of Phenytoin at Silica Surfaces, Mol. Pharm. 11 (2014) 610–616. https://doi.org/10.1021/mp4006479.
[7] D. Reischl, C. Röthel, P. Christian, E. Roblegg, H.M.A. Ehmann, I. Salzmann, O. Werzer, Surface-Induced Polymorphism as a Tool for Enhanced Dissolution: The Example of Phenytoin, Cryst. Growth Des. 15 (2015) 4687–4693. https://doi.org/10.1021/acs.cgd.5b01002.
[8] K. Tot, A. Lazić, B. Božić, A. Mandić, T.D. Sekulić, QSAR characterization of new synthesized hydantoins with antiproliferative activity, Biomed. Chromatogr. 33 (2019) e4539. https://doi.org/10.1002/bmc.4539.
[9] A.M.A. Aboeldahab, E.A.M. Beshr, M.E. Shoman, S.M. Rabea, O.M. Aly, Spirohydantoins and 1,2,4-triazole-3-carboxamide derivatives as inhibitors of histone deacetylase: Design, synthesis, and biological evaluation, Eur. J. Med. Chem. 146 (2018) 79–92. https://doi.org/10.1016/j.ejmech.2018.01.021.
[10] I. Gomez-Monterrey, G. Santelli, P. Campiglia, D. Califano, F. Falasconi, C. Pisano, L. Vesci, T. Lama, P. Grieco, E. Novellino, Synthesis and Cytotoxic Evaluation of Novel Spirohydantoin Derivatives of the Dihydrothieno[2,3-b]naphtho-4,9-dione System, J. Med. Chem. 48 (2005) 1152–1157. https://doi.org/10.1021/jm0408565.
[11] F. Wu, H. Jiang, B. Zheng, M. Kogiso, Y. Yao, C. Zhou, X.-N. Li, Y. Song, Inhibition of Cancer-Associated Mutant Isocitrate Dehydrogenases by 2-Thiohydantoin Compounds, J. Med. Chem. 58 (2015) 6899–6908. https://doi.org/10.1021/acs.jmedchem.5b00684.
[12] A.S. Guerra, D.J. Malta, L.P. Laranjeira, M.B. Maia, N.C. Colaço, C.L.M. De, S.L. Galdino, R.I. Pitta, T. Gonçalves-Silva, Anti-inflammatory and antinociceptive activities of indole-imidazolidine derivatives., Int. Immunopharmacol. 11 (2011) 1816–1822. https://doi.org/10.1016/j.intimp.2011.07.010.
[13] S.M. Sondhi, J. Singh, A. Kumar, H. Jamal, P.P. Gupta, Synthesis of amidine and amide derivatives and their evaluation for anti-inflammatory and analgesic activities, Eur. J. Med. Chem. 44 (2009) 1010–1015. https://doi.org/10.1016/j.ejmech.2008.06.029.
[14] N. Teno, K. Gohda, Y. Yamashita, T. Otsubo, M. Yamaguchi, K. Wanaka, Y. Tsuda, Plasmin inhibitors with hydrophobic amino acid-based linker between hydantoin moiety and benzimidazole scaffold enhance inhibitory activity, Bioorg. Med. Chem. Lett. 26 (2016) 2259–2261. https://doi.org/10.1016/j.bmcl.2016.03.047.
[15] N. Teno, K. Gohda, K. Wanaka, Y. Tsuda, T. Sueda, Y. Yamashita, T. Otsubo, Pyrrolopyrimidine-inhibitors with hydantoin moiety as spacer can explore P4/S4 interaction on plasmin, Bioorg. Med. Chem. 22 (2014) 2339–2352. https://doi.org/10.1016/j.bmc.2014.02.002.
[16] J. Handzlik, E. Szymańska, J. Chevalier, E. Otrębska, K. Kieć-Kononowicz, J.-M. Pagès, S. Alibert, Amine–alkyl derivatives of hydantoin: New tool to combat resistant bacteria, Eur. J. Med. Chem. 46 (2011) 5807–5816. https://doi.org/10.1016/j.ejmech.2011.09.032.

[17] D. Sergent, Q. Wang, N.A. Sasaki, J. Ouazzani, Synthesis of hydantoin analogues of (2S,3R,4S)-4-hydroxyisoleucine with insulinotropic properties, Bioorg. Med. Chem. Lett. 18 (2008) 4332–4335. https://doi.org/10.1016/j.bmcl.2008.06.081.
[18] N. Shankaraiah, S. Nekkanti, K.J. Chudasama, K.R. Senwar, P. Sharma, M.K. Jeengar, V.G.M. Naidu, V. Srinivasulu, G. Srinivasulu, A. Kamal, Design, synthesis and anticancer evaluation of tetrahydro-β-carboline-hydantoin hybrids, Bioorg. Med. Chem. Lett. 24 (2014) 5413–5417. https://doi.org/10.1016/j.bmcl.2014.10.038.
[19] H.U. Stilz, W. Guba, B. Jablonka, M. Just, O. Klingler, W. König, V. Wehner, G. Zoller, Discovery of an Orally Active Non-Peptide Fibrinogen Receptor Antagonist Based on the Hydantoin Scaffold, J. Med. Chem. 44 (2001) 1158–1176. https://doi.org/10.1021/jm001068s.
[20] M.J. Meyers, E.J. Anderson, S.A. McNitt, T.M. Krenning, M. Singh, J. Xu, W. Zeng, L. Qin, W. Xu, S. Zhao, L. Qin, C.S. Eickhoff, J. Oliva, M.A. Campbell, S.D. Arnett, M.J. Prinsen, D.W. Griggs, P.G. Ruminski, D.E. Goldberg, K. Ding, X. Liu, Z. Tu, M.D. Tortorella, F.M. Sverdrup, X. Chen, Evaluation of spiropiperidine hydantoins as a novel class of antimalarial agents., Bioorg. Med. Chem. 23 (2015) 5144–5150. https://doi.org/10.1016/j.bmc.2015.02.050.
[21] L.O. Olasunkanmi, B.P. Moloto, I.B. Obot, E.E. Ebenso, Anticorrosion studies of some hydantoin derivatives for mild steel in 0.5M HCl solution: Experimental, quantum chemical, Monte Carlo simulations and QSAR studies, J. Mol. Liq. 252 (2018) 62–74. https://doi.org/10.1016/j.molliq.2017.11.169.
[22] W. Guerrab, I.-M. Chung, S. Kansiz, J.T. Mague, N. Dege, J. Taoufik, R. Salghi, I.H. Ali, M.I. Khan, H. Lgaz, Synthesis, structural and molecular characterization of 2, 2-diphenyl-2H, 3H, 5H, 6H, 7H-imidazo [2, 1-b][1, 3] thiazin-3-one, J. Mol. Struct. 1197 (2019) 369–376.
[23] Y. Ramli, R. Akrad, W. Guerrab, J. Taoufik, M. Ansar, J.T. Mague, Ethyl 2-(2, 5-dioxo-4, 4-diphenylimidazolidin-1-yl) acetate, IUCrData. 2 (2017) x170098.
[24] Y. Ramli, W. Guerrab, A. Moussaif, J. Taoufik, E. Essassi, J. Mague, 3-[2-(5-Oxo-4, 4-diphenyl-2-sulfanylideneimidazolidin-1-yl) ethyl]-1, 3-oxazolidin-2-one, IUCrData. 2 (2017) x171041.
[25] R. Akrad, J.T. Mague, W. Guerrab, J. Taoufik, M. Ansar, Y. Ramli, 1-Benzyl-2-benzylsulfanyl-4, 4-diphenyl-4, 5-dihydro-1H-imidazol-5-one, IUCrData. 2 (2017) x170033.
[26] G.M. Sheldrick, SHELXT: Integrating space group determination and structure solution, Acta Crystallogr Sect Found Adv. 70 (2014) C1437.
[27] L. Krause, R. Herbst-Irmer, D. Stalke, An empirical correction for the influence of low-energy contamination, J. Appl. Crystallogr. 48 (2015) 1907–1913.
[28] S. Parsons, H.D. Flack, T. Wagner, Use of intensity quotients and differences in absolute structure refinement, Acta Crystallogr. Sect. B Struct. Sci. Cryst. Eng. Mater. 69 (2013) 249–259.
[29] A. Frisch, gaussian 09W Reference, Wallingford USA 25p. (2009).
[30] R. Dennington, T. Keith, J. Millam, GaussView, Version 4.1. 2, Semichem Inc Shawnee Mission KS. (2007).
[31] A.D. Becke, Density-functional exchange-energy approximation with correct asymptotic behavior, Phys. Rev. A. 38 (1988) 3098.
[32] A.D. Becke, A new mixing of Hartree–Fock and local density-functional theories, J. Chem. Phys. 98 (1993) 1372–1377.
[33] A.D. Becke, Becke's three parameter hybrid method using the LYP correlation functional, J Chem Phys. 98 (1993) 5648–5652.
[34] J.P. Perdew, K. Burke, M. Ernzerhof, Generalized gradient approximation made simple, Phys. Rev. Lett. 77 (1996) 3865.
[35] D. Studio, Accelrys Inc, San Diego CA USA. (2013).
[36] K.C. Prathap, N. Lokanath, Three novel coumarin-benzenesulfonylhydrazide hybrids: Synthesis, characterization, crystal structure, Hirshfeld surface, DFT and NBO studies, J. Mol. Struct. (2018).

[37] K.O. Rachedi, T.-S. Ouk, R. Bahadi, A. Bouzina, S.-E. Djouad, K. Bechlem, R. Zerrouki, T. Ben Hadda, F. Almalki, M. Berredjem, Synthesis, DFT and POM analyses of cytotoxicity activity of α-amidophosphonates derivatives: Identification of potential antiviral O,O-pharmacophore site, J. Mol. Struct. 1197 (2019) 196–203. https://doi.org/10.1016/j.molstruc.2019.07.053.

[38] S. Uzun, Z. Esen, E. Koç, N.C. Usta, M. Ceylan, Experimental and density functional theory (MEP, FMO, NLO, Fukui functions) and antibacterial activity studies on 2-amino-4- (4-nitrophenyl) -5,6-dihydrobenzo [h] quinoline-3-carbonitrile, J. Mol. Struct. 1178 (2019) 450–457. https://doi.org/10.1016/j.molstruc.2018.10.001.

[39] R.I. Al-Wabli, K.S. Resmi, Y. Sheena Mary, C. Yohannan Panicker, M.I. Attia, A.A. El-Emam, C. Van Alsenoy, Vibrational spectroscopic studies, Fukui functions, HOMO-LUMO, NLO, NBO analysis and molecular docking study of (E)-1-(1,3-benzodioxol-5-yl)-4,4-dimethylpent-1-en-3-one, a potential precursor to bioactive agents, J. Mol. Struct. 1123 (2016) 375–383. https://doi.org/10.1016/j.molstruc.2016.07.044.

[40] N.A. Ancın, S.G. Öztaş, Ö. Küçükterzi, N.A. Öztaş, Theoretical investigation of N-trans-cinnamylidene-m-toluidine by DFT method and molecular docking studies, J. Mol. Struct. 1198 (2019) 126868. https://doi.org/10.1016/j.molstruc.2019.07.115.

[41] S. Sakthivel, T. Alagesan, S. Muthu, C.S. Abraham, E. Geetha, Quantum mechanical, spectroscopic study (FT-IR and FT - Raman), NBO analysis, HOMO-LUMO, first order hyperpolarizability and docking studies of a non-steroidal anti-inflammatory compound, J. Mol. Struct. 1156 (2018) 645–656. https://doi.org/10.1016/j.molstruc.2017.12.024.

[42] Y. Oueslati, S. Kansız, A. Valkonen, T. Sahbani, N. Dege, W. Smirani, Synthesis, crystal structure, DFT calculations, Hirshfeld surface, vibrational and optical properties of a novel hybrid non-centrosymmetric material (C10H15N2) 2H2P2O7, J. Mol. Struct. 1196 (2019) 499–507.

[43] N. Islam, S. Kaya, Conceptual Density Functional Theory and Its Application in the Chemical Domain, CRC Press, 2018.

[44] G. Serdaroğlu, J. Ortiz, Ab initio calculations on some antiepileptic drugs such as phenytoin, phenbarbital, ethosuximide and carbamazepine, Struct. Chem. 28 (2017) 957–964.

[45] M.E. Mashuga, L.O. Olasunkanmi, E.E. Ebenso, Experimental and theoretical investigation of the inhibitory effect of new pyridazine derivatives for the corrosion of mild steel in 1 M HCl, J. Mol. Struct. 1136 (2017) 127–139. https://doi.org/10.1016/j.molstruc.2017.02.002.

[46] Ş. Erdoğan, Z.S. Safi, S. Kaya, D.Ö. Işın, L. Guo, C. Kaya, A computational study on corrosion inhibition performances of novel quinoline derivatives against the corrosion of iron, J. Mol. Struct. 1134 (2017) 751–761. https://doi.org/10.1016/j.molstruc.2017.01.037.

[47] H. Shokry, Molecular dynamics simulation and quantum chemical calculations for the adsorption of some Azo-azomethine derivatives on mild steel, J. Mol. Struct. 1060 (2014) 80–87. https://doi.org/10.1016/j.molstruc.2013.12.030.

[48] P.K. Chattaraj, U. Sarkar, D.R. Roy, Electrophilicity index, Chem. Rev. 106 (2006) 2065–2091.

[49] R.G. Parr, L. v Szentpaly, S. Liu, Electrophilicity index, J. Am. Chem. Soc. 121 (1999) 1922–1924.

[50] L.H. Madkour, S. Kaya, L. Guo, C. Kaya, Quantum chemical calculations, molecular dynamic (MD) simulations and experimental studies of using some azo dyes as corrosion inhibitors for iron. Part 2: Bis–azo dye derivatives, J. Mol. Struct. 1163 (2018) 397–417. https://doi.org/10.1016/j.molstruc.2018.03.013.

[51] W. Guerrab, I.-M. Chung, S. Kansiz, J.T. Mague, N. Dege, J. Taoufik, R. Salghi, I.H. Ali, M.I. Khan, H. Lgaz, Synthesis, structural and molecular characterization of 2, 2-diphenyl-2H, 3H, 5H, 6H, 7H-imidazo [2, 1-b][1, 3] thiazin-3-one, J. Mol. Struct. 1197 (2019) 369–376.

[52] B.A. Nogueira, G.O. Ildiz, J. Canotilho, M.E.S. Eusebio, R. Fausto, Molecular structure, infrared spectra, photochemistry, and thermal properties of 1-methylhydantoin, J. Phys. Chem. A. 118 (2014) 5994–6008.
[53] B.A. Nogueira, G. Ildiz, J. Canotilho, M. Eusébio, M. Henriques, J. Paixao, R. Fausto, 5-methylhydantoin: from isolated molecules in a low-temperature argon matrix to solid state polymorphs characterization, J. Phys. Chem. A. 121 (2017) 5267–5279.
[54] A. Dutta, S.Kr. Saha, P. Banerjee, D. Sukul, Correlating electronic structure with corrosion inhibition potentiality of some bis-benzimidazole derivatives for mild steel in hydrochloric acid: Combined experimental and theoretical studies, Corros. Sci. 98 (2015) 541–550. https://doi.org/10.1016/j.corsci.2015.05.065.
[55] H. Lgaz, I.-M. Chung, R. Salghi, I.H. Ali, A. Chaouiki, Y. El Aoufir, M.I. Khan, On the understanding of the adsorption of Fenugreek gum on mild steel in an acidic medium: Insights from experimental and computational studies, Appl. Surf. Sci. 463 (2019) 647–658. https://doi.org/10.1016/j.apsusc.2018.09.001.
[56] H. Mi, G. Xiao, X. Chen, Theoretical evaluation of corrosion inhibition performance of three antipyrine compounds, Comput. Theor. Chem. 1072 (2015) 7–14. https://doi.org/10.1016/j.comptc.2015.08.023.
[57] S.Kr. Saha, P. Ghosh, A. Hens, N.C. Murmu, P. Banerjee, Density functional theory and molecular dynamics simulation study on corrosion inhibition performance of mild steel by mercapto-quinoline Schiff base corrosion inhibitor, Phys. E Low-Dimens. Syst. Nanostructures. 66 (2015) 332–341. https://doi.org/10.1016/j.physe.2014.10.035.
[58] C. Morell, A. Grand, A. Toro-Labbé, Theoretical support for using the Δf (r) descriptor, Chem. Phys. Lett. 425 (2006) 342–346.
[59] Y.B. Shankar Rao, M.V.S. Prasad, N. Udaya Sri, V. Veeraiah, Vibrational (FT-IR, FT-Raman) and UV–Visible spectroscopic studies, HOMO–LUMO, NBO, NLO and MEP analysis of Benzyl (imino (1H-pyrazol-1-yl) methyl) carbamate using DFT calculaions, J. Mol. Struct. 1108 (2016) 567–582. https://doi.org/10.1016/j.molstruc.2015.12.008.
[60] Y.S. Mary, C.Y. Panicker, M. Sapnakumari, B. Narayana, B.K. Sarojini, A.A. Al-Saadi, C. Van Alsenoy, J.A. War, FT-IR, NBO, HOMO–LUMO, MEP analysis and molecular docking study of 1-[3-(4-Fluorophenyl)-5-phenyl-4,5-dihydro-1H-pyrazol-1-yl]ethanone, Spectrochim. Acta. A. Mol. Biomol. Spectrosc. 136, Part B (2015) 483–493. https://doi.org/10.1016/j.saa.2014.09.061.
[61] R. Yankova, S. Genieva, N. Halachev, G. Dimitrova, Molecular structure, vibrational spectra, MEP, HOMO-LUMO and NBO analysis of Hf(SeO3)(SeO4)(H2O)4, J. Mol. Struct. 1106 (2016) 82–88. https://doi.org/10.1016/j.molstruc.2015.10.091.
[62] R. Ilmi, S. Kansız, N. Dege, M.S. Khan, Synthesis, structure, Hirshfeld surface analysis and photophysical studies of red emitting europium acetylacetonate complex incorporating a phenanthroline derivative, J. Photochem. Photobiol. Chem. 377 (2019) 268–281.
[63] S. Kansız, A. Tolan, H. İçbudak, N. Dege, Synthesis, crystallographic structure, theoretical calculations, spectral and thermal properties of trans-diaquabis (trans-4-aminoantipyrine) cobalt (II) acesulfamate, J. Mol. Struct. 1190 (2019) 102–115.

Figure Captions

Figure 1. The title molecule with labeling scheme and 50% probability ellipsoids.

Figure 2. A portion of one hydrogen bonded chain viewed along the a-axis direction. N—H···O and C—H···O hydrogen bonds are shown, respectively, by blue and black dashed lines.

Figure 3. Packing viewed along the c-axis direction with the C—H···π(ring) interactions shown as green dashed lines.

Figure 4. Optimized molecular structure of 3-allyl-5,5-diphenylimidazolidine-2,4-dione obtained by DFT.

Figure 5. Frontier molecular orbitals (HOMO-LUMO) of 3-allyl-5,5-diphenylimidazolidine-2,4-dione.

Figure 6. The molecular electrostatic potential map of 3-allyl-5,5-diphenylimidazolidine-2,4-dione.

Figure 7. The view of the three-dimensional Hirshfeld surface of 3-allyl-5,5-diphenylimidazolidine-2,4-dione plotted over d_{norm} in the range -0.5973 to 1.5340 a.u..

Figure 8. The two-dimensional fingerprint plots for 3-allyl-5,5-diphenylimidazolidine-2,4-dione, showing (*a*) all interactions, (*b*) H···H, (*c*) C···H/H···C and (*d*) O···H/H···O interactions.

Fig. 1.

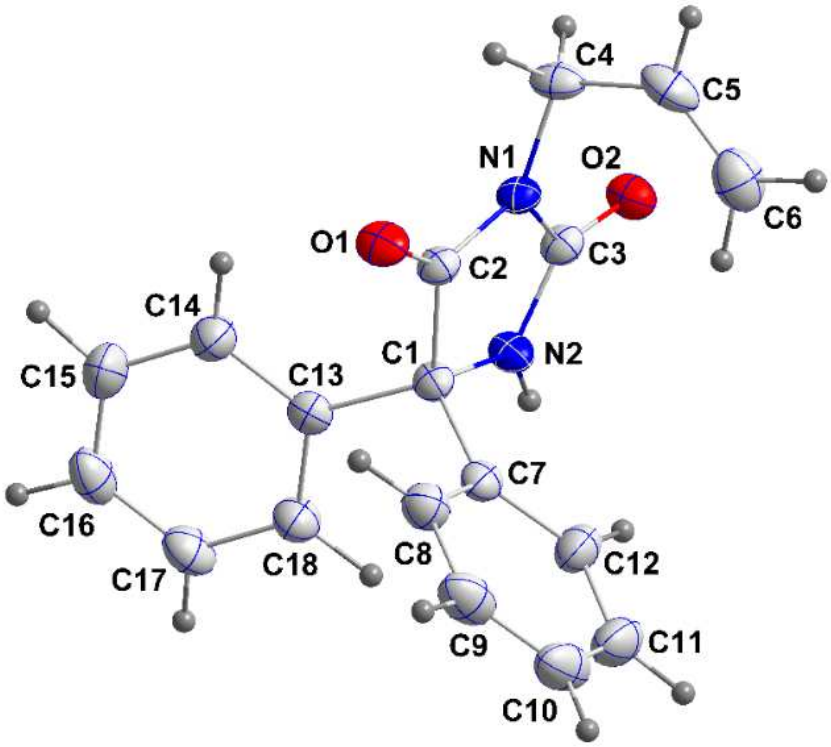

Fig. 2

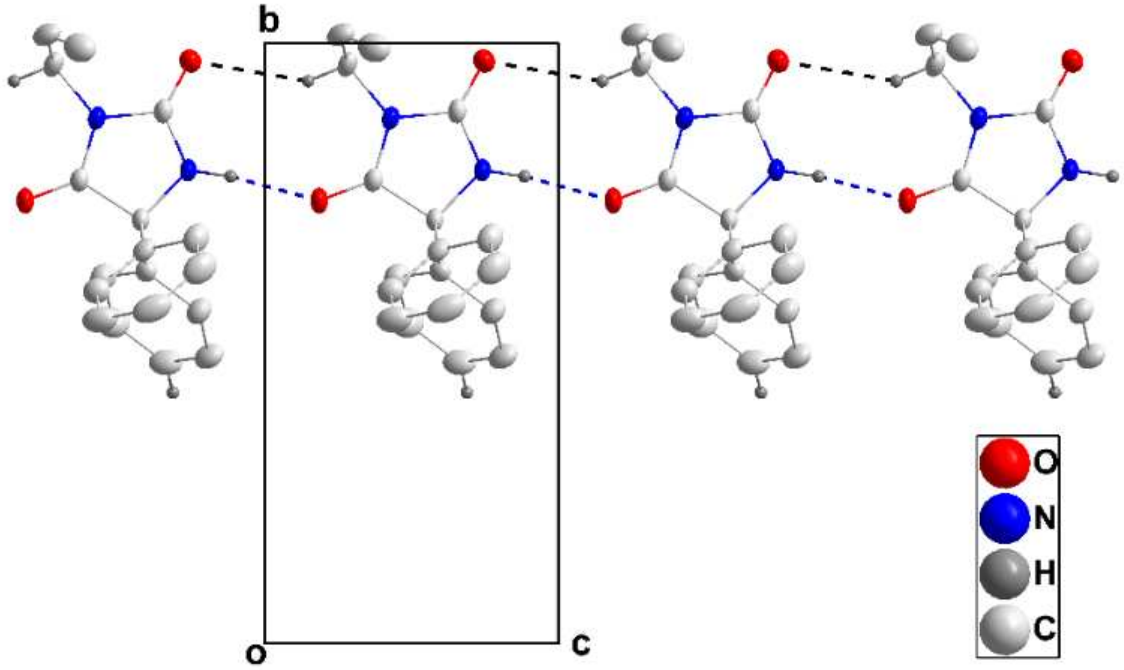

Fig. 3

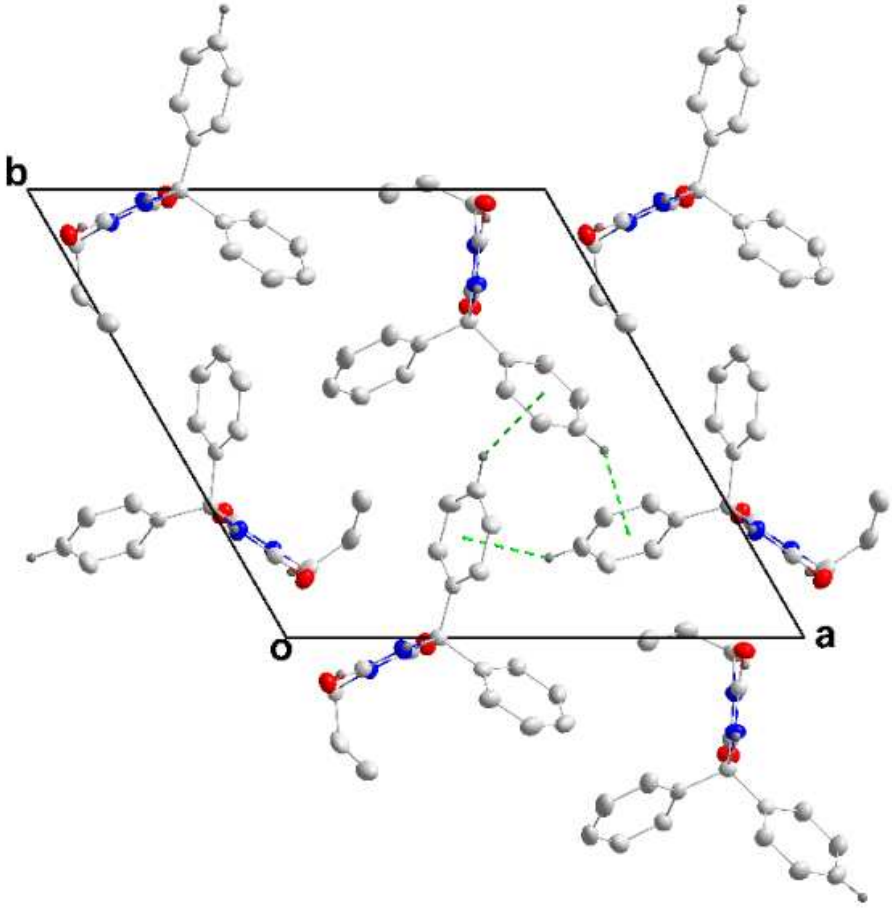

Fig. 4.

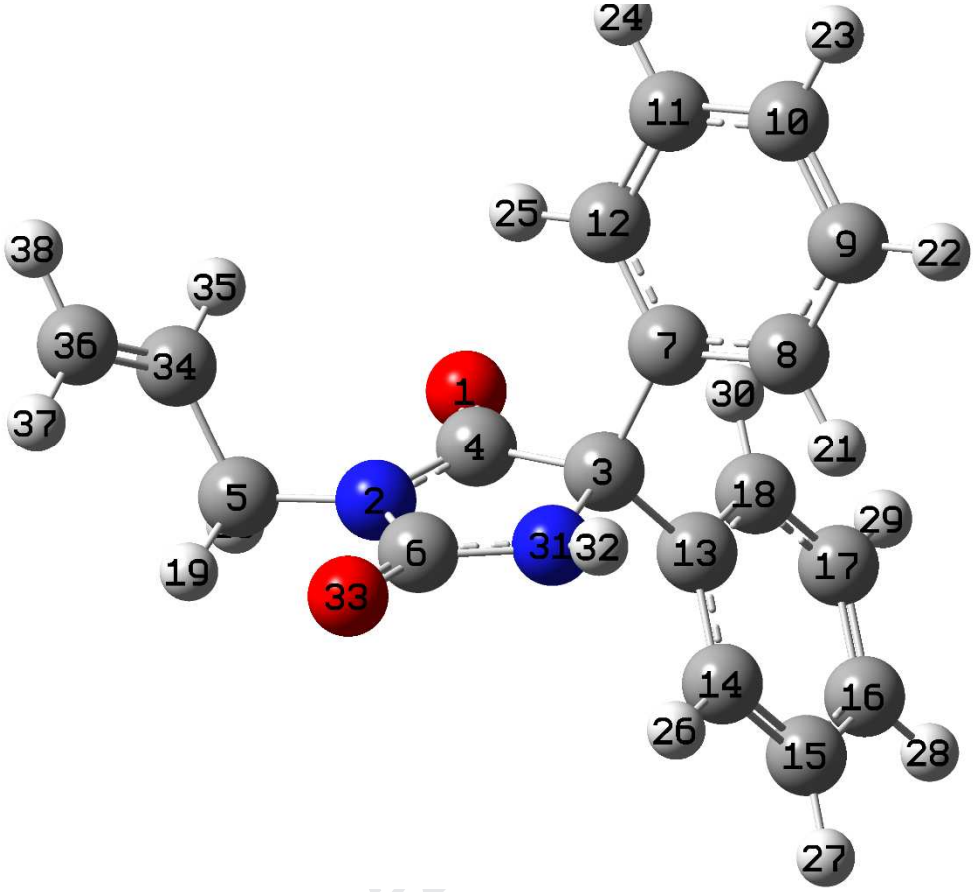

Fig. 5.

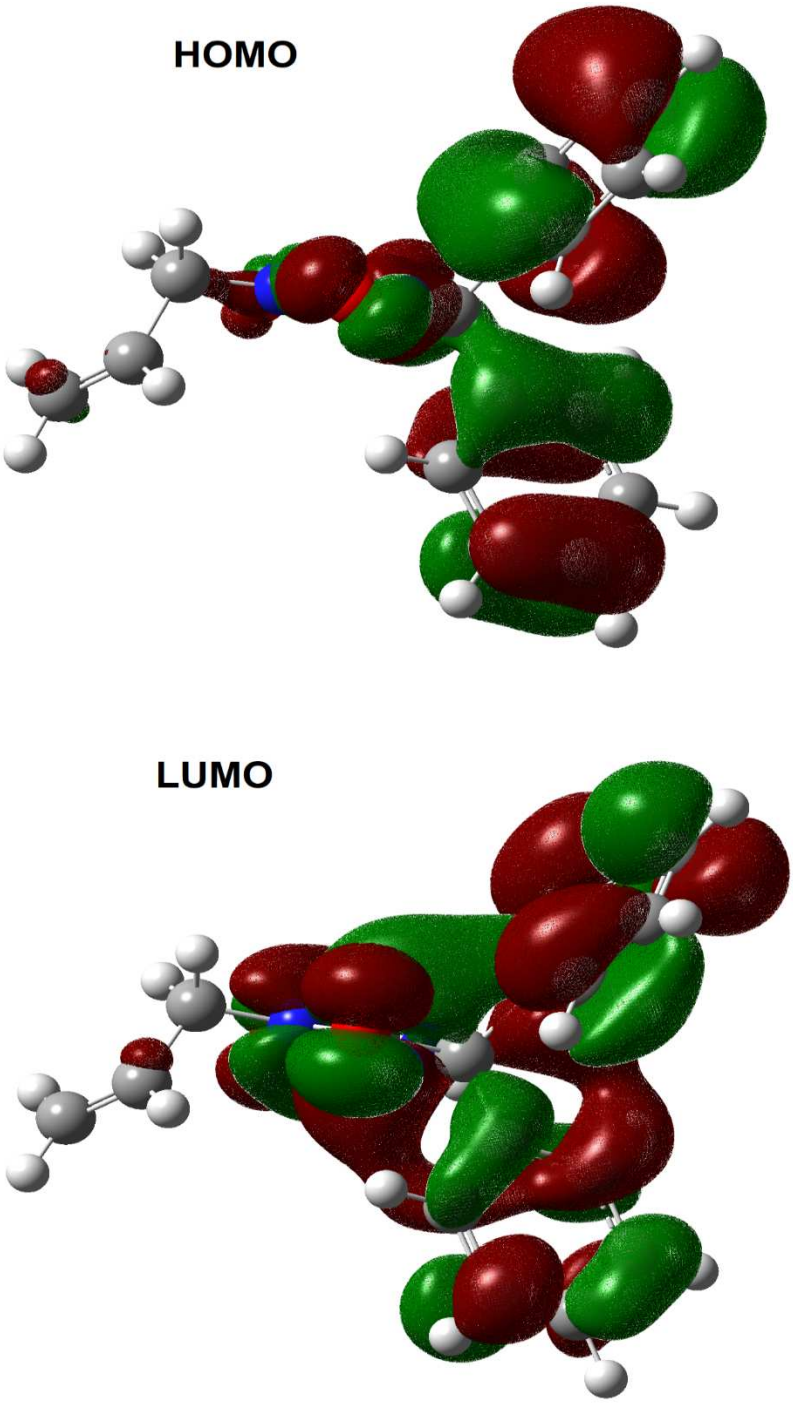

Fig. 6.

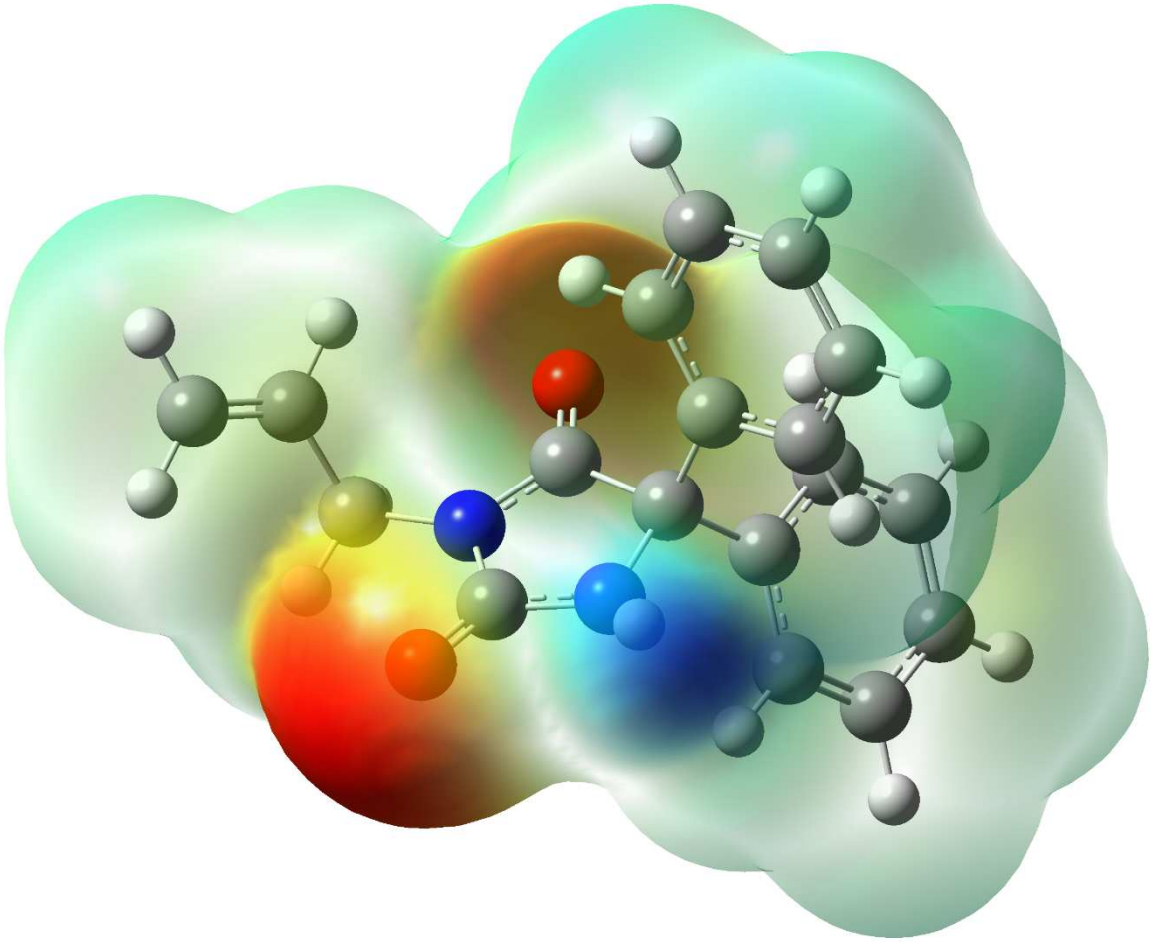

Fig. 7.

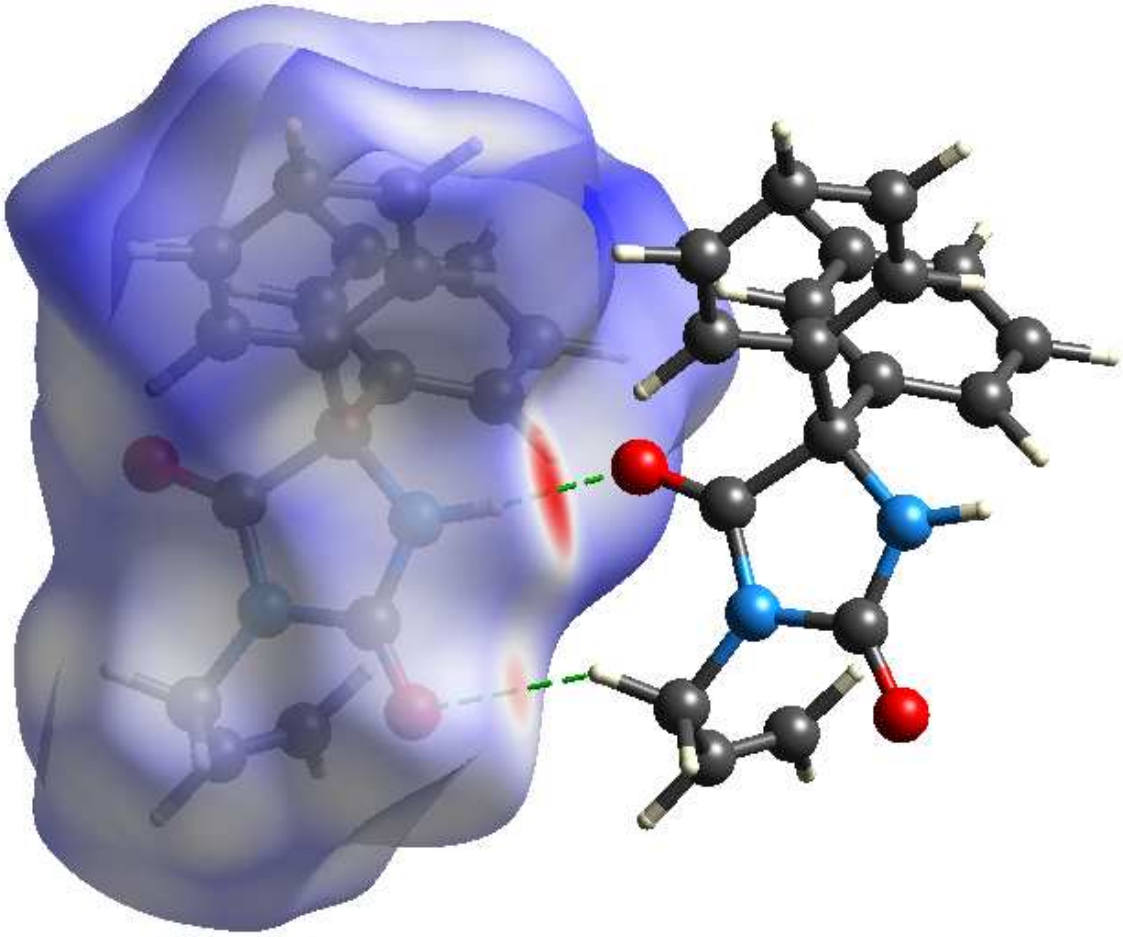

Fig. 8

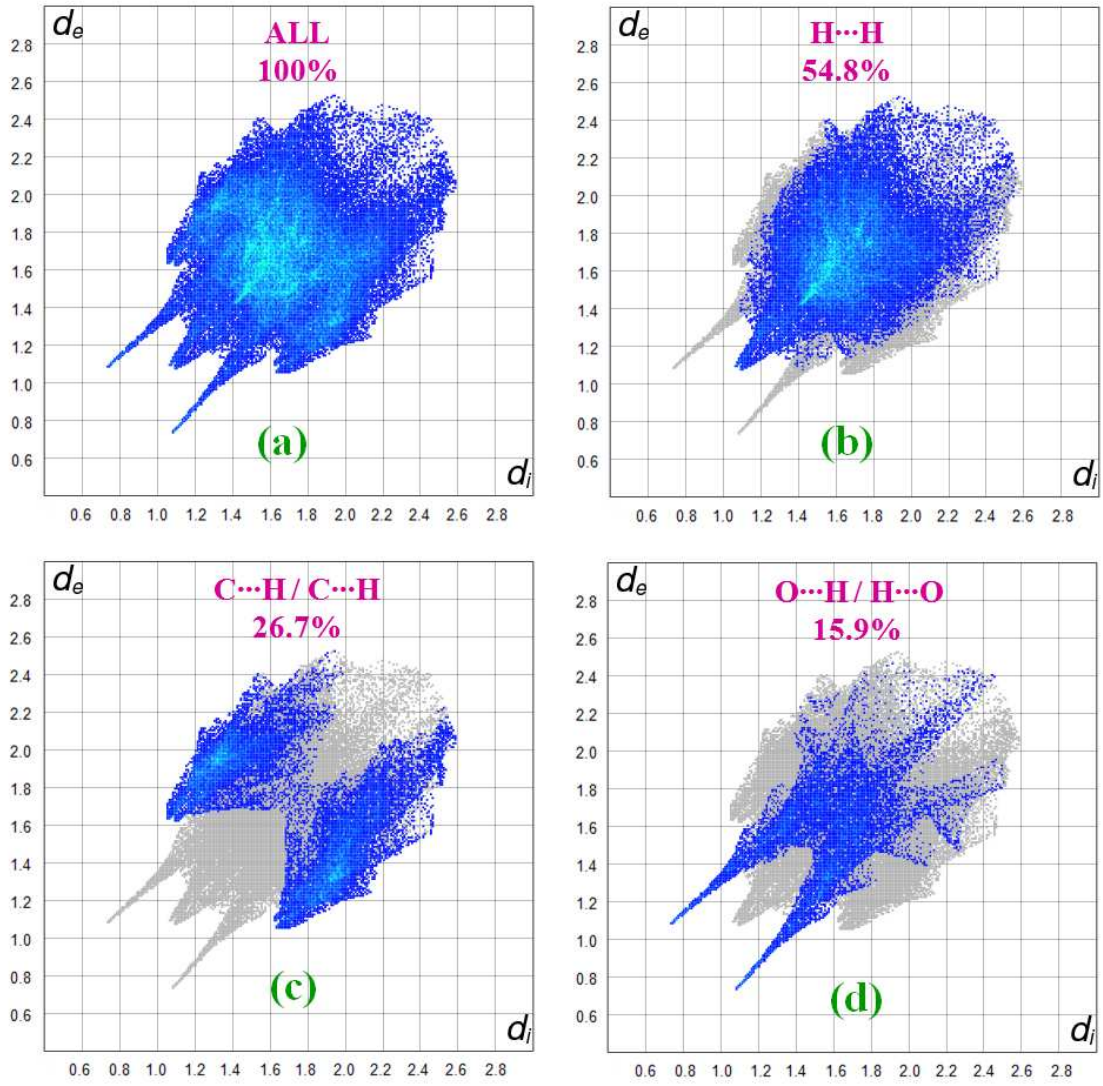
d_e
ALL
100%
(a)
d_i
H···H
54.8%
(b)
C···H / C···H
26.7%
(c)
O···H / H···O
15.9%
(d)
0.6 0.8 1.0 1.2 1.4 1.6 1.8 2.0 2.2 2.4 2.6 2.8

- 3-allyl-5,5-diphenylimidazolidine-2,4-dione has been synthesized and characterized by XRD.
- DFT, NBO and Fukui function analysis have been carried out.
- The XRD parameters were compared with the theoretical data.
- Hirshfeld surface analysis of crystal structure was studied.

Author Contributions Section:

Walid Guerrab, Hassane Lgaz, and M. Ansar: Performed experiments and calculations, analyzed the data, and wrote the initial manuscript.

Riadh Marzouki and Ismat H. Ali: Contributed data or analysis tools, formal analysis, resources, review&editing.

Sevgi Kansiz and Necmi Dege: Contributed data or analysis tools, review&editing.

Joel T. Mague: Contributed data or analysis tools, review&editing.

Youssef Ramli, Jamal Taoufik, and Ill-Min Chung: Conceptualization, methodology, supervision, review&editing.

All authors read and approved the manuscript.

Conflict of interest:

The authors of this manuscript have no conflict of interest to declare.